CHAPTER 13

MÖSSBAUER SPECTROSCOPY IN BIOLOGICAL AND BIOMEDICAL RESEARCH

ALEXANDER A. KAMNEV,[1] KRISZTINA KOVÁCS,[2] IRINA V. ALENKINA,[3] AND MICHAEL I. OSHTRAKH[3]

[1]*Laboratory of Biochemistry, Institute of Biochemistry and Physiology of Plants and Microorganisms, Russian Academy of Sciences, Saratov, Russian Federation*
[2]*Laboratory of Nuclear Chemistry, Institute of Chemistry, Eötvös Loránd University, Budapest, Hungary*
[3]*Faculty of Physical Techniques and Devices for Quality Control, Institute of Physics and Technology, Ural Federal University, Ekaterinburg, Russian Federation*

13.1 INTRODUCTION

Modern approaches aimed at studying physiological and pathological processes in living systems require applications of physical techniques that can provide information at the molecular level. Mössbauer spectroscopy was already used for investigating biological materials a few years after the discovery of Rudolf Mössbauer. The development of biological applications paved the way for further applications of Mössbauer spectroscopy in medical research. Therefore, the term "biomedical" can be considered both from a broader viewpoint, which means all possible aspects of biological research, and from a narrower viewpoint, which means any biological, biophysical, and biochemical research related to medical problems (normal and pathological physiology, environmental factors and health, medicine and pharmaceutics, etc.) [1]. In this chapter, the latter meaning of the term "biomedical research" will be used, in addition to biological studies.

Up to now, several thousand papers on various biological aspects of Mössbauer spectroscopy applications have been published (for some previous reviews see, for instance, Refs. 2–12), while only about 350–400 articles can be considered as biomedical from the narrower viewpoint (for reviews see Refs. 13–25). These studies were based mainly on ^{57}Fe-containing subjects; however, in a number of cases, ^{57}Co, ^{119}Sn, ^{129}I, ^{153}Sm, ^{161}Tb, and ^{197}Au containing species were used. Various objects, from molecules to tissues and organs, were studied in normal physiological conditions and in the case of pathologies.

In this chapter, some recent examples of biology-related and biomedical applications of Mössbauer spectroscopy are considered, including studies related to microorganisms, plants, iron-containing biomolecules, tissues, and pharmaceutical products. Attention is also paid to different Mössbauer techniques involving the usual transmission geometry (emission experiments recently discussed in Refs. 26–30 will be reviewed separately [31]) and newly developed Mössbauer spectroscopy with a high velocity resolution [32,33]. The first results of biomedical applications of Mössbauer spectroscopy with a high velocity resolution were reviewed in Refs. 34–39 and are briefly considered within this chapter, while applications of Mössbauer spectroscopy using synchrotron radiation were recently reviewed in Refs. 12,40.

Mössbauer Spectroscopy: Applications in Chemistry, Biology, and Nanotechnology, First Edition.
Edited by Virender K. Sharma, Gostar Klingelhofer, and Tetsuaki Nishida.
© 2013 John Wiley & Sons, Inc. Published 2013 by John Wiley & Sons, Inc.

UNCORRECTED PROOF

CH13 07/04/2013 8:10:49 Page 273

13.2 MICROORGANISMS-RELATED STUDIES

Microorganisms in soil and aquifers are well documented to be actively involved in a range of biogeochemical processes leading to biomineralization and in a diversity of chemical transformations of soil minerals. Fe(III), largely represented by extremely poorly water-soluble oxyhydroxides of variable crystallinity, is an essential component of many soil minerals. A variety of soil bacteria were reported to couple oxidation of soil organic matter, including organic pollutants, to dissimilatory reduction of many redox-active metals, primarily Fe(III) and Mn(IV) [41].

Besides the above-described directly biotic reduction of Fe(III) by microbial cells, a range of secondary metabolites, produced both by soil microorganisms and by plant roots and excreted into the environment, can abiotically reduce Fe (III). Some earlier and more recent experiments using ^{57}Fe Mössbauer spectroscopy have shown that such biologically and environmentally important low molecular weight organic substances as anthranilic (*o*-aminobenzoic) acid [42,43], indolic compounds including tryptophan, indole-3-acetic acid (IAA, a phytohormone of the auxin series produced by many soil microorganisms), and other auxins [44–50], cysteine (e.g., adsorbed on clay) [51], and so on, can abiotically reduce Fe(III) in weakly acidic media (under pH 4–5) even under aerobic conditions.

Note that in the case of tryptophan, no Fe(III) reduction was observed within 15 min after mixing the reagents even at pH ~2 [46], while the resulting Fe(II) had earlier been detected in Mössbauer spectra after longer periods [49,50]. In particular, partial reduction of Fe(III) to Fe(II) was detected by Mössbauer spectroscopy in the course of synthesis of ferric complexes with tryptophan and lysine, which included the procedures of precipitation and extraction with nonaqueous solvents [49].

Gradual Fe(III) reduction to Fe(II) by a series of auxins (indole-3-alkanoic acids with C_1–C_4 side chains) in weakly acidic aqueous solutions was evident from Mössbauer spectroscopic measurements [46,47] performed in rapidly frozen solutions after 15 min and 2 days of reaction at ambient temperature (Fig. 13.1). In that case, rapid freezing allows all the ongoing processes to be ceased at a certain time point, and Mössbauer measurements in the solidified frozen matrix become feasible.

Already 15 min after mixing ^{57}Fe(III) salt solution with that of an organic acid, high-spin Fe(II) was readily detectable in the spectra of filtered and frozen solutions by its characteristic quadrupole doublet with a large value of quadrupole splitting. After 2 days under those conditions, Fe(II) dominated in all the solutions, except for indole-3-carboxylic acid (ICA) (see Fig. 13.1e) for which the reduction rate was definitely lower than that for the other indolic acids studied. In all the cases (see Fig. 13.1), the Fe(II) quadrupole doublets gave the following parameters: isomer shift (δ), ~1.40 mm s^{-1}

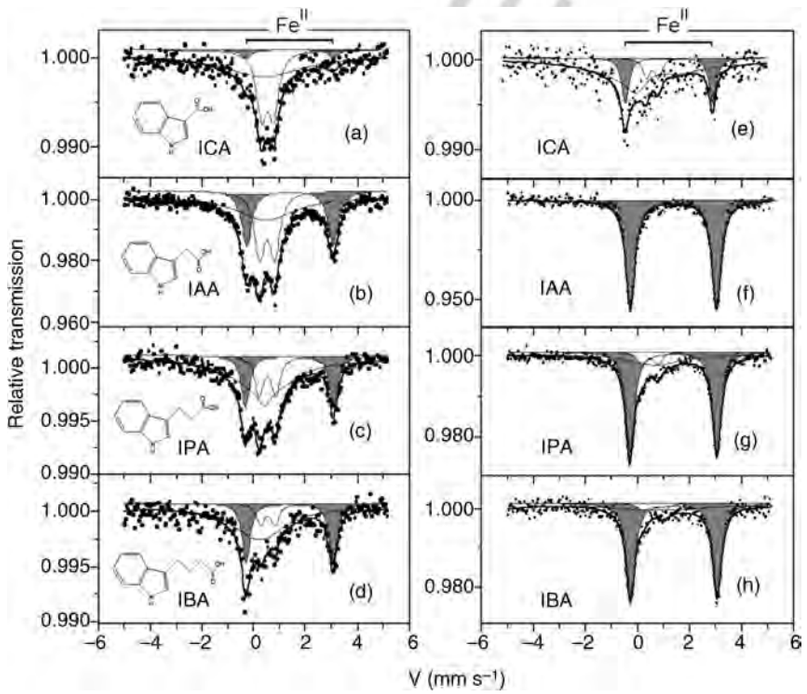

FIGURE 13.1

Mössbauer spectra of mixed ^{57}Fe(III) nitrate and indole-3-alkanoic acid aqueous solutions (molar ratios 1:3; initial ^{57}Fe(III) concentration 0.01 M) filtered and rapidly frozen (at T = 80 K) 15 min (a–d) and 2 days (e–h) after mixing the reagents (final pH ~3). Acids used: (a), (e)—ICA; (b), (f)—IAA; (c), (g)—indole-3-propionic acid (IPA); (d), (h)—indole-3-butyric acid (IBA). The position of the components related to Fe(II) (shaded areas) is shown in the upper plots by square brackets. (Adapted from Refs. 46, 47.)

CH13 07/04/2013 8:10:49 Page 274

(here and further δ for ^{57}Fe are given relative to α-Fe at 295 K); quadrupole splitting (ΔE_Q), 3.3 mm s^{-1} (at $T = 80$ K), which corresponds to ferrous hexaaquo complex [52]. Thus, the reduced iron ions in the solutions were most probably in the hydrated form not coordinated to the acids or their oxidation products.

It is noteworthy that for indole-3-acetic acid, a virtually full reduction was observed within 2 days (see Fig. 13.1f), which corresponds to its more easily proceeding oxidative decarboxylation [41]. However, after drying the mixture in air, all the Fe(II) was found to get reoxidized back to Fe(III) [44]. This effect, under appropriate soil conditions (acidic medium, varying humidity), could give rise to a cycling process facilitating oxidative degradation of IAA in soil in the presence of Fe(III) [44,45]. Since acidic soils are rather widely distributed, besides highly metal-polluted soils that often have lower pH [41], such abiotic Fe(III) reduction involving organic molecules of biotic origin may significantly contribute to iron transformation in soil [41,49].

Another representative ecologically important example of Fe(III) redox interaction with microbially produced extracellular biomolecules involves alkylresorcinols with short alkyl side chains—microbial signaling molecules that have been documented to perform autoregulatory and adaptogenic functions under unfavorable conditions and show other remarkably diverse biochemical and physiological activities [53]. In aqueous mixtures of 5-methylresorcinol and ^{57}Fe(III) salt at final pH ~3, the appearance of Fe(II) was clearly detectable by Mössbauer spectroscopy (at 80 K) already in a few

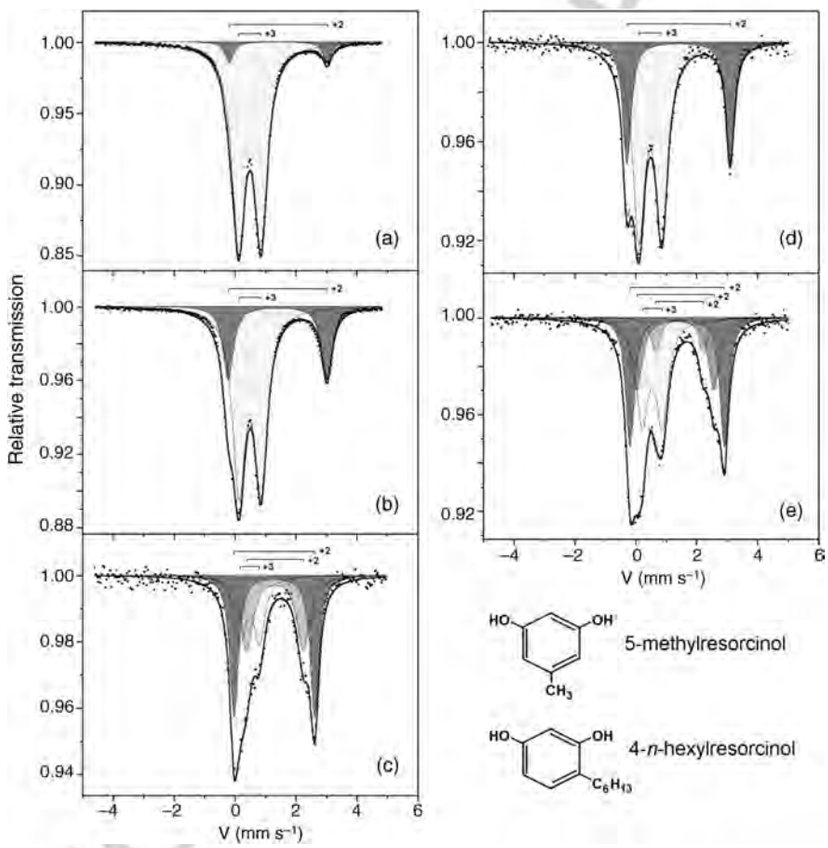

FIGURE 13.2

Mössbauer spectra of ^{57}Fe(III)-containing aqueous solutions (a) of 5-methylresorcinol (orcinol) rapidly frozen 10 min and (b) 5.5 h after mixing (final pH ~3), as well as of (c) the solid residue obtained by air-drying the mixture at room temperature; (d) of ^{57}Fe(III)-containing aqueous (20% (v/v) ethanol) solution of 4-*n*-hexylresorcinol rapidly frozen 5 min after mixing (final pH ~3) and (e) of the solid residue obtained by air-drying the mixture at room temperature (initial molar Fe-to-alkylresorcinol ratios 1:3; initial ^{57}Fe(III) concentration 0.016 M); all spectra measured at T = 80 K. The shaded areas (quadrupole doublets) represent contributions of Fe(III) (the most lightly shaded area) or Fe(II) (darker shaded areas) to the whole spectrum area (defined by the outer solid-line envelope); in spectra (c) and (e), the two and three darker-shaded areas, respectively, correspond to two different Fe(II) forms (see Table 13.1). The position of each quadrupole doublet is shown by a square bracket above the spectra, with indication of the corresponding Fe oxidation state. (Adapted from Ref. 53.)

CH13 07/04/2013 8:10:50 Page 275

TABLE 13.1 Mössbauer Parameters for ^{57}Fe(III)-Containing Aqueous Solutions of 5-Methylresorcinol and 4-*n*-Hexylresorcinol (Containing 20% (v/v) Ethanol; see also Fig. 13.2) at pH ~3 (Total [Fe] = 16 ± 1 mM; 1:3 Fe-to-Alkylresorcinol Molar Ratios), Rapidly Frozen After Specified Periods of Time, and for Their Solid Residues Obtained by Drying in Air at Ambient Temperature (Measured at T = 80 K) [53]

Alkylresorcinol Mixed with ^{57}Fe(III) in Solution *(Sample Measured)*	Time[a]	Fe Oxidation State	δ [b, c] (mm s^{-1})	ΔE_Q [c, d] (mm s^{-1})	Γ_{exp} [c, e] (mm s^{-1})	S[f] (%)
5-Methylresorcinol (*solution*)	10 min	+3	0.48(1)	0.74(1)	0.52(1)	93.3
		+2	1.41(1)	3.22(1)	0.34(1)	6.7
	5.5 h	+3	0.48(1)	0.72(1)	0.50(1)	74.1
		+2	1.38(1)	3.23(1)	0.42(1)	25.9
5-Methylresorcinol (*dried solid*)	–	+3	0.48(1)	0.63(2)	0.43(2)	24.5
		+2 (*form 1*)	1.31(1)	1.86(3)	0.50(3)	33.3
		+2 (*form 2*)	1.29(1)	2.65(1)	0.34(1)	42.2
4-*n*-Hexylresorcinol (*solution*)	5 min	+3	0.475(3)	0.757(4)	0.49(1)	68.8
		+2	1.402(3)	3.388(5)	0.34(1)	31.2
4-*n*-Hexylresorcinol (*dried solid*)	–	+3	0.54(1)	0.65(1)	0.48(2)	34.9
		+2 (*form 1*)	1.43(1)	1.55(3)	0.35(3)	9.0
		+2 (*form 2*)	1.29(1)	2.54(2)	0.45(3)	23.7
		+2 (*form 3*)	1.359(3)	3.10(1)	0.34(1)	32.4

[a]Period from mixing the reagents until rapid freezing of the solution.
[b]Isomer shift (relative to α-Fe at ambient temperature).
[c]Errors (in the last digits) obtained from the fits are given in parentheses.
[d]Quadrupole splitting.
[e]Full line width at half maximum.
[f]Relative SD are within ca. ±4%.

minutes (Fig. 13.2a), while its gradual accumulation was evident within a few hours after mixing (Fig. 13.2b; all the Mössbauer parameters evaluated from the spectra are listed in Table 13.1). The parameters of the ferrous species formed upon Fe(III) reduction in the solutions (in particular, $\delta \sim 1.4$ mm s^{-1}; $\Delta E_Q \sim 3.2$ mm s^{-1} at $T = 80$ K) most closely correspond to hexaaquo Fe(II) coordination [52,54].

Drying the mixture of 5-methylresorcinol and Fe(III) in air under ambient conditions led to the resulting dried solid that gave a more complicated Mössbauer spectrum (Fig. 13.2c), with two different forms of Fe(II) species (altogether comprising over three-fourth of the total iron), along with a residual ferric form (see Table 13.1). The parameters of the two ferrous forms evidently represent different complexes of Fe(II) with the possible residuary 5-methylresorcinol and/or its oxidation product(s) that might include 1,2,3-trihydroxy- and/or 1,3,4-trihydroxy-5-methylbenzenes, or the relevant hydroxylated quinones [53]. Thus, those Mössbauer measurements, in line with the UV spectroscopic monitoring of the soluble products [55], provide clear evidence that Fe(III) is gradually reduced by 5-methylresorcinol in moderately acidic (pH ~3) aqueous solutions in air.

Interestingly, under the same conditions, 4-*n*-hexylresorcinol showed a significantly higher Fe(III) reduction rate. Already 5 min after mixing the reagents, about a third of the total Fe(III) was reduced to Fe(II) represented by a quadrupole doublet with the parameters typical for hexaaquo Fe(II) complex (Fig. 13.2d; see also Table 13.1). As Fe(III) ions at pH ~3 are well known to be prone to hydrolytic polymerization, in this case the residual Fe(III), which gives virtually the same Mössbauer parameters as those for the aqueous 5-methylresorcinol solution 10 min after mixing, represents, most probably, hydrolyzed polymeric and/or colloidal hydroxo species [52]. Note that some participation of the organic molecules or their oxidation products in Fe(III) coordination cannot be ruled out merely on the basis of Fe(III) Mössbauer parameters.

After similarly drying the mixture of 4-*n*-hexylresorcinol and Fe(III) in air under ambient conditions, the resulting dried solid gave a yet more complicated Mössbauer spectrum, with three different forms of ferrous species (altogether comprising ca. two-third of the total iron), along with a residual ferric form (Fig. 13.2e; see also Table 13.1). The parameters of the ferrous forms in the dry residue, except probably for form 3 (which are rather close to those for hydrated Fe^{2+} ions in solid ferrous chloride hydrates at $T \sim 80$ K [52]), evidently correspond to different Fe(II) complexes with the possible residuary 4-*n*-hexylresorcinol and/or its oxidation product(s). However, note that these parameters and, consequently, the Fe^{2+} microenvironments (i.e., type and arrangement of donor atoms in the ligands) differ from those for the dried 5-methylresorcinol solution (see above and Table 13.1). Different positions of the alkyl substituents in the 1,3-dihydroxybenzene (i.e., resorcinol) moieties might be expected to lead to different oxidation products of the

UNCORRECTED PROOF

CH13 07/04/2013 8:10:50 Page 276

5- and 4-alkylsubstituted resorcinols [55]. This factor, possibly together with the length of the alkyl group, might be a reason for the significant difference in the Fe(III) reduction rate observed for 5-methyl- (i.e., 5-C_1-alkyl; a gradual redox process) and 4-*n*-hexyl-substituted resorcinol (4-*n*-C_6-alkyl; a much more rapid redox process). Similar trends of Fe(III) reduction in going from the autoinducer solutions to their air-dried solids have also been obtained at slightly lower pH ~1.5 [53].

The redox behavior of Fe(III) mixtures with both alkylresorcinols [53,55] upon drying was totally different from that of indole-3-acetic acid (auxin) aqueous solutions studied earlier [44,45]. In the latter case, all Fe(II) formed had been found to get reoxidized back to Fe(III). In contrast, in dried solutions of the alkylresorcinols, the resulting Fe(II) was not reoxidized upon drying in air; moreover, it was in fact found to be dominating in the dried solid (see Table 13.1). These findings point to significantly stronger reducing and/or binding (coordinating) power of alkylresorcinols or their oxidation products as compared to those of auxin.

The aforementioned examples unambiguously imply that some microbial autoinducers can be abiotically oxidized by soil Fe(III) in moderately acidic media, which is of ecological significance with regard to microbial signaling. An oxidation process involving a particular molecular signal is very likely to exclude the latter from any signaling pathways, which is equal to "message undelivery", directly affecting microbial autoregulation and, generally, intercellular communication in the microbial consortium.

Mössbauer spectroscopy has been applied to microbial biomineralization studies in a few recent reports. For the anaerobic alkaliphilic dissimilatory Fe(III)-reducing bacterium *Geoalkalibacter ferrihydriticus*, reduction of amorphous ferric hydroxide (AFH), coupled to acetate oxidation [56,57], led to the formation of siderite $FeCO_3$ (at low AFH concentrations) and poorly (under [AFH] ~0.07 M) or better crystallized magnetically ordered phases (at [AFH] above 0.07 M). The analysis of Mössbauer spectra using hyperfine field distributions demonstrated that the distribution with a lower isomer shift value ($\delta \sim 0.3\ \mathrm{mm\,s^{-1}}$) could be attributed to cations Fe^{3+} located in A-positions of magnetite Fe_3O_4 and in both positions of maghemite γ-Fe_2O_3 while that with a large isomer shift value ($\delta \sim 0.6\ \mathrm{mm\,s^{-1}}$) could be attributed to cations $Fe^{2.5+}$ located in the B-positions of magnetite [57]. It was also shown that anthraquinone-2,6-disulfonate (quinone, an additional "electron shuttle") added to the bacterial cultivation medium resulted in a more intensive AFH reduction, increasing the relative content of Fe_3O_4 and siderite [57]. The intensity of the magnetically split sextet increased with an increase in the quinone concentration up to $C_q \sim 0.05\ \mathrm{g\,l^{-1}}$; remaining unchanged up to $C_q = 0.3\ \mathrm{g\,l^{-1}}$. The relaxation character of the Mössbauer spectra became more pronounced for $C_q \geq 0.4\ \mathrm{g\,l^{-1}}$, reflecting a reduction in the superparamagnetic particle size.

Using temperature-dependent Mössbauer measurements (at 4.5–300 K), a similar AFH reduction was reported [58] by a binary bacterial culture including, besides *G. ferrihydriticus*, also the non-Fe(III)-reducing alkaliphilic bacterium *Anaerobacillus alkalilacustre* (in the presence of mannitol as the only substrate). The reduction process takes place due to the growth of the former bacterium that utilizes the metabolic products formed by the latter that fermented mannitol.

Fe(III) mineral characterization was reported using Mössbauer spectroscopy and X-ray diffraction for minerals formed in cell suspensions of *Acidovorax* sp. BoFeN1, a nitrate-reducing, Fe(II)-oxidizing bacterium [59]. Lepidocrocite (γ-FeOOH) (90%), which also forms after Fe(II) chemical oxidation by dissolved O_2, and goethite (α-FeOOH) (10%) were produced at pH 7.0 in the absence of strongly complexing ligands. Higher pH, increasing concentrations of carbonate or humic acids promoted goethite formation and caused little or no changes in Fe(II) oxidation rates; phosphate resulted in the formation of unidentifiable Fe(III) solids and notably slowed Fe(II) oxidation rates. Fe(III) mineralogy due to bacterial Fe(II) oxidation thus seems to be strongly influenced by the solution chemistry.

Using Mössbauer spectroscopy, three positions of trivalent iron with nonoverlapping ranges of ΔE_Q were revealed in bacterial ferrihydrite nanoparticles, produced by the bacterium *Klebsiella oxytoca* in the course of biomineralization of iron salt solutions from a natural medium, after sample heating [60]. The fit of these spectra and interpretation of results seem to be doubtful, as the authors did not take into account a complicated iron core structure in bacterial ferritin and a core size variation while relating their results to merely two structural differences in ferrihydrite.

In the magnetotactic bacterium *Magnetospirillum gryphiswaldense*, Mössbauer spectroscopic measurements allowed a mechanism to be proposed for initial magnetite formation via membrane-bound ferritin and an Fe(II) species at the cytoplasmic membrane [61]. The iron required for magnetite biomineralization is released directly at the membrane invagination pit interface without iron flux via the cytoplasm. This might imply distinct transport pathways for Fe_3O_4 formation and biochemical utilization of iron.

13.3 PLANTS

Although Mössbauer spectroscopy is capable of selectively characterizing Fe-containing chemical species, there have been relatively few Mössbauer spectroscopic studies of iron in intact plant tissues. This is mainly because of the special

CH13 07/04/2013 8:10:51 Page 277

sample requirements for obtaining an adequate Mössbauer spectrum. The biggest constraint is a very low iron content in plants (and a low natural abundance of ^{57}Fe). In addition, for the observation of the Mössbauer effect, the sample should be in a solid state.

Despite these limitations, the technique has been applied in the past to characterize the forms of iron occurring in different plants [62–65]. More recently, a detailed study of iron uptake and translocation in rice [66] grown in anaerobic $^{57}FeCl_2$-enriched nutrient solutions showed primarily the presence of Fe(III) hydrous oxide components precipitated on the root cell wall (ferrihydrite and/or lepidocrocite). No evidence of Fe(II) was found in the leaf tissue, the spectra were characteristic of Fe(III) present in ferritin and in other complexed forms, not further identified by the authors. Iron biomineralization was also observed in a perennial grass grown in extreme acidic environment with a high content of metals [67,68]. In this case, the Mössbauer spectral analysis indicated that iron accumulated in this plant mainly as jarosite and ferrihydrite (ferritin). Jarosite accumulated in roots and rhizomes, while ferritin was detected in all the structures.

Iron is an essential nutrient for plants and crucial for a variety of cell functions. In most soils, iron is not readily available for plants due to the low solubility of iron oxyhydroxides at the soil pH. For this reason, plants have evolved different strategies for iron uptake. Nongraminaceous plants follow strategy I that starts with reduction of iron chelates at the outer surface of the plasma membrane [65,69]. The plasma membrane-bound enzyme, ferric reductase oxidase 2, was shown to accept Fe(III) chelates and use cytoplasmic reducing equivalents ($FADH_2$[1] or NADPH[2]) to reduce them to Fe(II) chelate [70] that releases iron due to its much lower stability, and the ferrous ions are taken up by a divalent cation transporter. The reduction rate is increased under iron deficiency and is also accompanied by an increased proton release [69]. In contrast, graminaceous monocots can produce phytosiderophores—specific, low molecular weight Fe (III)-binding polydentate organic ligands—which solubilize iron and make it available for absorption (strategy II iron uptake mechanism), that was earlier analyzed in [65].

In absorbing different species, such as Fe(III) or Fe(II), both the cell membrane and the cell wall play an important role. The complex network of cell walls within the whole plant organism is called the apoplast. It promotes the contact of cells with the environment and forms an internal space for the nonphysiological accumulation of ionic and uncharged particles. After the iron is taken up through the membranes, it enters the cytoplasm, that builds a continuous network called symplast, through microscopic channels between the cells. The targets of iron assimilation are different enzymes and structures. Among these, heme proteins, iron–sulfur proteins and phytoferritin should be mentioned.

Roots of Fe-sufficient cucumber (*Cucumis sativus*) were grown in hydroponic culture in unbuffered, modified Hoagland solution containing 10 μM $^{57}Fe(III)$ citrate [71–73]. The Mössbauer spectrum (Fig. 13.3a), recorded at $T = 80$ K, of the iron-sufficient cucumber root grown with 10 μM $^{57}Fe(III)$ citrate, shows an envelope of wide symmetrical quadrupole doublet that can represent several Fe(III) microenvironments. Basing on the spectral components assigned in the Mössbauer studies of plants [62,63,66,67], the spectra were fitted with three symmetrical doublets. The main component denoted by $Fe(III)_A$ represented an iron species in an octahedral coordination with $\delta = 0.50\,\text{mm s}^{-1}$, $\Delta E_Q = 0.44\,\text{mm s}^{-1}$, and its relative area (S) 44%. The $Fe(III)_B$ component had $\delta = 0.50\,\text{mm s}^{-1}$, $\Delta E_Q = 0.80\,\text{mm s}^{-1}$, and $S = 35\%$. The third component, $Fe(III)_C$ ($S = 21\%$), had $\delta = 0.50\,\text{mm s}^{-1}$, $\Delta E_Q = 1.22\,\text{mm s}^{-1}$ [73]. The Mössbauer spectrum of the freeze-dried cucumber root (Fig. 13.3b) [74] recorded at 4.2 K exhibited a ~70% magnetically split subspectrum, while one of the three doublet components, existing at higher temperatures, disappeared. At 1.5 K, almost all species were magnetically ordered (Fig. 13.3c). The remaining paramagnetic species represented by the quadrupole doublet could be transformed into magnetically split spectrum by applying 5 T external magnetic field (Fig. 13.3d). The Mössbauer parameters obtained from the fit in the case of the iron-sufficient cucumber show that the major component in the roots is a high-spin Fe(III) in octahedral coordination ($Fe(III)_A$) possibly resulting from Fe(III)–carboxylate complexes. These carboxylate complexes may include Fe(III)–organic acid and Fe(III)–amino acid species inside the cell and Fe(III)–pectates in the apoplast. The Mössbauer parameters of the $Fe(III)_B$ component are in good agreement with those reported for ferrihydrite in ferritin found in several plant tissues, for example, in pea roots [63], or in rice [66]. The third doublet with the highest quadrupole splitting ($Fe(III)_C$) can represent sulfate–hydroxide containing Fe(III) species. According to its characteristic Mössbauer parameters, it can be attributed to jarosite [67,75] or its analogous compound $(MFe_3(OH)_6(SO_4)_2$, $M = K^+$, H_3O^+, Na^+, …). It should be noted that another explanation of several quadrupole doublets required for the best fit of Mössbauer spectra of ferritin iron cores will be considered further in Section 13.6.

However, it was not possible (not even with the help of the low-temperature measurements) to identify unequivocally which compounds are represented by $Fe(III)_B$ and $Fe(III)_C$, since the magnetic ordering temperatures

[1] 1,5-Dihydro flavin adenine dinucleotide.
[2] Reduced form of nicotinamide dinucleotide phosphate.

CH13 07/04/2013 8:10:51 Page 278

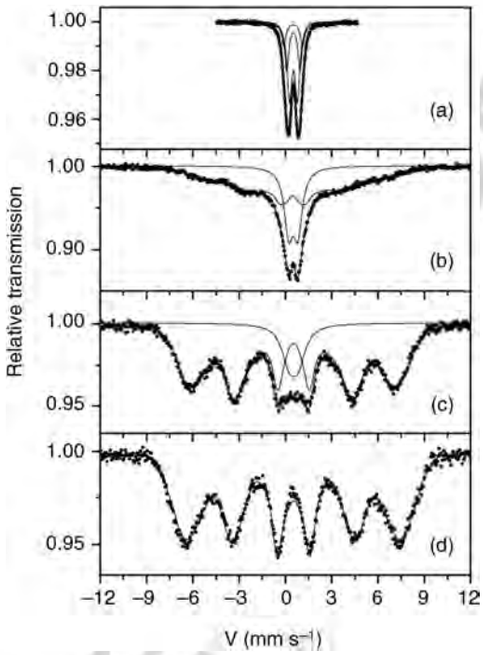

FIGURE 13.3

Mössbauer spectra of iron-sufficient cucumber roots grown in 10 μM ^{57}Fe(III)-citrate-containing nutrient solution recorded at (a) T = 80 K; (b) T = 4.2 K; (c) T = 1.5 K; (d) T = 1.5 K applying 5 T external magnetic field perpendicular to the propagation of the γ-ray. (Adapted from Refs. 72,73.)

strongly depend on the particle sizes and crystallinity of the Fe(III) aggregates and are in strong correlation with the stoichiometry of these compounds [63,72,76]. The magnetic properties of hydrous ferric oxides formed via biomineralization processes (as in the case of the iron-storage protein ferritin) also strongly depend on its composition [76]. The high PO_4^{3-} ratio and the incorporation of organic ions such as citrate can lead to an amorphous structure and to a decrease in the antiferromagnetic ordering temperature (<4 K). Considering that the iron uptake in strategy I-type plants is accompanied by a significant proton release and that a high amount of sulfate ions is present in the nutrient solution, the formation of sulfate–hydroxide containing Fe(III) species with various stoichiometry can be favored in the cell wall. These findings support that the magnetically split subspectra at 4.2 and 1.5 K can be attributed to Fe(III) hydroxosulfates and hydrous ferric oxides, respectively. However, the interpretation of the magnetically split subspectrum for one superparamagnetic Fe-rich phase, such as ferritin with a small number of Fe atoms in the clusters, probably containing other ligands such as PO_4^{3-}, SO_4^{2-}, and organic acids, cannot be entirely excluded. The paramagnetic component, which can be transformed to magnetically split spectrum by applying 5 T external magnetic field at 1.5 K, supports the presence of ferric carboxylates, since the parameters of the quadrupole doublet ($\delta = 0.5$ mm s^{-1}, $\Delta E_Q = 0.6$ mm s^{-1}), presented in Fig. 13.3b,c at 4.2 and 1.5 K, correspond to those of the Fe(III)$_A$ component.

Although cucumber belongs to strategy I group, no Fe(II) could be detected when enough iron was available for the plant, which is in good agreement with the previous Mössbauer results. This can be explained by the high relative amount of Fe(III) present in the root tissues of iron-sufficient plants (suppressing the small contribution of the possible Fe(II) in the Mössbauer spectrum). Three main types of iron-bearing species were suggested (sulfate–hydroxide containing ferric species in the apoplast, hydrous ferric oxides possibly present as ferritin inside the cell, and Fe(III) carboxylate complexes both in the symplast and apoplast) to be formed naturally in the roots of cucumber grown in unbuffered Fe(III)–citrate nutrient solution.

Cucumbers were grown in iron-deficient nutrient solutions and supplied with ^{57}Fe(III) citrate at different concentrations (10, 50, 100, and 500 μM) for 30 min and at 500 μM for different time intervals (30, 60, 90, 180 min, and 24 h) only before harvest. Mössbauer spectra of the cucumber roots taken after iron supply ($T = 80$ K) are shown in Fig. 13.4 [73,77]. The Mössbauer spectra of iron-deficient cucumber roots supplied with 500 μM ^{57}Fe(III) citrate for 30 min could be decomposed similar to the iron-sufficient samples, but in this case, an Fe(II) component could also be found besides the Fe(III)$_A$ and Fe(III)$_C$ components (Fe(III)$_B$ did not appear in this case). The relative amounts of the different iron species depended on the duration of iron supply (Table 13.2) [73]: the Fe(II) showed a significant decrease with the iron treatment, while the relative amount of the total Fe(III) increased. Application of different iron concentrations during iron supply in 30-min time interval did not change the components that can be assigned to

CH13 07/04/2013 8:10:51 Page 279

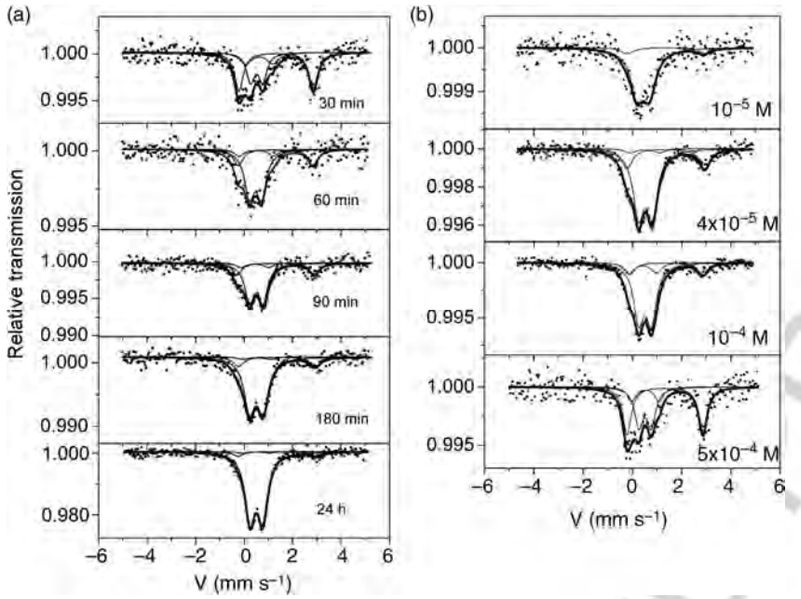

FIGURE 13.4
Mössbauer spectra (recorded at T = 80 K) of iron-deficient cucumber roots, supplied with 500 μM ^{57}Fe(III) citrate for different time periods, as indicated in the Figure (a) [77], and supplied with different ^{57}Fe(III) citrate concentrations, as indicated in the Figure, for 30 min (b) [73].

the Mössbauer spectra of iron-deficient plants supplied with 500 μM ^{57}Fe(III) citrate. As can be seen from Fig. 13.4, the relative amount of the detected Fe(II) showed a correlation with the concentration of the iron present in the nutrient solution (Table 13.2). With increasing the amount of Fe(III) citrate, the amount of the reduced iron increased as well.

The fact that iron(II) was clearly detected by Mössbauer spectroscopy gives a direct evidence for the iron uptake mechanism of strategy I. As the time of the iron treatment increased, the reductive capacity was decreasing because of the increased amount of iron already taken up by the root [73]. According to the Mössbauer parameters of the Fe(II), one can see that it formed a hexaaquo complex [52] that might be the primary hydrated product of the ferric chelate reductase enzyme, accumulated in the apoplast and not attached to any of the cell wall components. At the same time, the increase in the $Fe(III)_A$ component, representing iron both attached to the apoplast and taken up inside the cell, could be observed. The ferritin-like component (denoted by $Fe(III)_B$) was absolutely not detectable, which means this duration of

TABLE 13.2 Mössbauer Parameters of the Iron Components Found in the Iron Deficient Cucumber Roots that were Supplied with 500 μM ^{57}Fe(III) Citrate for Different Time Intervals and with Different Amounts of ^{57}Fe(III) Citrate for 30 min [73]

	Fe(II) Component			$Fe(III)_A$ Component			$Fe(III)_C$ Component		
Sample	δ_1[e] (mm s^{-1})	ΔE_{Q1}[e] (mm s^{-1})	S_1[f] (%)	δ_2[e] (mm s^{-1})	ΔE_{Q2}[e] (mm s^{-1})	S_2[f] (%)	δ_3[e] (mm s^{-1})	ΔE_{Q3}[e] (mm s^{-1})	S_3[b] (%)
Different time intervals during iron supply									
30 min	1.35	3.19	48	0.49	0.46	32	0.52	1.11	20
60 min	1.31	3.05	23	0.46	0.44	60	0.45	1.15	17
90 min	1.30	3.19	23	0.50	0.50	69	0.44	1.14	9
180 min	1.35	3.17	15	0.50	0.48	81	0.50	1.14	4
24 h	1.37	3.23	6	0.51	0.52	91	0.47	1.12	3
Different iron concentrations during iron supply									
10^{-5} M	1.31	3.22	13	0.43	0.50	87	–	–	–
5×10^{-5} M	1.35	3.15	23	0.52	0.55	72	0.50	1.23	5
10^{-4} M	1.36	2.96	16	0.51	0.51	71	0.43	1.09	13
5×10^{-4} M	1.35	3.19	48	0.49	0.46	32	0.52	1.11	20

[a]SD $\leq$ 0.05 mm s^{-1}.
[b]Relative SD $\leq$ 5%.

UNCORRECTED PROOF

CH13 07/04/2013 8:10:52 Page 280

iron supply was insufficient for producing the iron-storage protein. The accumulation of the iron/sulfate–hydroxide component was possibly also not favored in this case, since $Fe(III)_C$ showed a decreasing tendency.

Similar results were shown by different iron concentrations applied during iron supply but more information could be obtained about the mechanism of the reduction and the iron uptake. The relatively low amount of Fe(II) in the case of the lowest applied $^{57}Fe(III)$ citrate concentration (see Fig. 13.4) can be explained by a very fast uptake and reoxidation process. If more Fe(III) was available, the Fe(II)/Fe(III) ratio was shown to increase. Consequently, the accumulation of Fe (II) in the apoplast was favored because of limited uptake and/or reoxidation processes. Comparing the total iron concentration in the root with the amount reducible in 30 min [73], it can be assumed that the reduction rate was high enough to potentially reduce all Fe accumulated in the apoplast. Concerning that the uptake rate of Fe(II) is limited, this might result in the accumulation of Fe(II) outside the plasma membrane.

13.4 ENZYMES

Many excellent applications of Mössbauer spectroscopy to heme and nonheme iron-containing metalloproteins were reviewed in earlier reports (Section 13.1). A more recent "forum" article by Krebs et al. [78] should be mentioned. With an introduction to the technique, it then focuses on recent developments pertaining to the application of ^{57}Fe Mössbauer spectroscopy in biochemistry, including the rapid freeze-quench method in conjunction with Mössbauer spectroscopy to monitor changes at the Fe-containing active site during a biochemical reaction. Nowadays, annually there appear numerous publications on such fascinating topics involving Mössbauer spectroscopy (often accompanied by other techniques). A few representative examples briefly considered below give a general view of its capabilities.

Iron–sulfur clusters are versatile electron transfer cofactors, which are ubiquitous in many metalloenzymes. In the *Bacillus subtilis*, redox regulator (Fnr) that controls genes of the anaerobic metabolism in response to low oxygen tension, an unusual structure for the oxygen-sensing $[4Fe\text{-}4S]^{2+}$ cluster was detected by a combination of genetic experiments with UV–visible and Mössbauer spectroscopy [79]. Asp-141 was identified as the fourth iron–sulfur cluster ligand besides three Cys residues.

In the oxygen-tolerant [NiFe] hydrogenase from the hyperthermophilic bacterium *Aquifex aeolicus*, three iron–sulfur clusters were identified in their usual redox states, a [3Fe-4S] and two [4Fe-4S], but also a unique high-potential state was found [80]. On the basis of ^{57}Fe Mössbauer spectroscopy, this high-potential form was attributed to a superoxidized state of the [4Fe-4S] center proximal to the [NiFe] site. The unique environment of this cluster, characterized by a surplus cysteine coordination, is able to tune the redox potentials and make it compliant with the $[4Fe\text{-}4S]^{3+}$ state. It is actually the first example of a biological [4Fe-4S] center that physiologically switches between $3+$, $2+$, and $1+$ oxidation states within a very small potential range.

Nonheme Fe is a conservative component of the Q-type photosynthetic reaction centers but its function remains unknown. Using Mössbauer spectroscopy, it was shown [81] that in *Rhodospirillum rubrum* the nonheme Fe exists mostly in a ferrous low-spin state. The binding of Cd^{2+} ions in the vicinity of the quinone–Fe complex changed the high-spin state of the nonheme Fe into a low-spin one characterized by hyperfine parameters similar to those obtained for the nonheme Fe low-spin state in untreated reaction centers, as confirmed by Mössbauer measurements.

A homologue of the ferric uptake regulator (Fur) in *M. gryphiswaldense* was identified and analyzed in [82]. A fur deletion mutant of *M. gryphiswaldense* biomineralized fewer and slightly smaller magnetite crystals than did the wild type. Although the total cellular iron accumulation of the mutant was decreased owing to reduced magnetite biomineralization, it exhibited an increased level of free intracellular iron, which was bound mostly to a ferritin-like metabolite that was found significantly increased in Mössbauer spectra of the mutant.

The rapid-quench method [78] was used in Ref. 83 to analyze the mechanism of a bacterial phenylalanine hydroxylase, a mononuclear nonheme iron protein that uses tetrahydropterin as the source of the two electrons needed to activate O_2 for the hydroxylation of phenylalanine to tyrosine. Mössbauer spectra of samples prepared by freeze-quenching the reaction of the complex enzyme–$^{57}Fe(II)$–phenylalanine–6-methyltetrahydropterin with O_2 revealed the accumulation of an intermediate at short reaction times (20–100 ms). The Mössbauer parameters of the intermediate ($\delta = 0.28\,mm\,s^{-1}$, $\Delta E_Q = 1.26\,mm\,s^{-1}$) suggested it to be a high-spin Fe(IV) complex similar to those that have previously been detected in the reactions of other mononuclear Fe(II) hydroxylases.

Low-temperature molecular dynamics simulations of cytochrome *c* oxidase were used in Ref. 84 to predict an experimentally observable Mössbauer spectral width. Predicted lineshapes were used to model Lorentzian doublets, with which published cytochrome *c* oxidase Mössbauer spectra were simulated. Molecular dynamics-imposed

CH13 07/04/2013 8:10:52 Page 281

constraints to spectral lineshapes allowed useful information to be obtained, for example, the presence of multiple chemical species in the binuclear center of cytochrome *c* oxidase. Molecular dynamics-based predictions were found to be in good agreement with published experimental spectra [84], showing promise for a renewed interest for application of this approach in bioenergetics.

13.5 HEMOGLOBIN

Hemoglobin is the iron-containing oxygen-transport heme protein. Vertebrate hemoglobins are tetramers consisting of two pairs of nonidentical protein chains (for review see Refs. 85,86). Human and animal adult hemoglobins consist of two α-subunits and two β-subunits. Each subunit binds heme (iron protoporphyrin IX complex) that is the active site of hemoglobin. Heme Fe(II) reversibly binds an oxygen molecule to realize protein function. Myoglobin, an oxygen-storage heme protein, is similar to β-chains.

Owing to the important role of the heme iron electronic structure in the process of reversible oxygen binding, Mössbauer spectroscopy of hemoglobins was related to the studies of the heme iron electronic structure variations in relation to the heme iron stereochemistry. These studies were based on some features of Mössbauer spectra of hemoglobins. It was observed that Mössbauer spectra of tetrameric oxyhemoglobin had a non-Lorentzian line shape in the liquid nitrogen temperature region [87–90]. This asymmetry was better fitted using a superposition of two quadrupole doublets. It was supposed that two quadrupole doublets may be a result of the heme iron electronic structure nonequivalence in α- and β-subunits of oxyhemoglobin. Further analysis of Mössbauer spectra of oxy-, deoxy-, and carboxyhemoglobins [90,91] as well as theoretical quantum chemical calculations of quadrupole splitting for the deoxyheme models in different subunits [92–94] demonstrated the necessity of taking into account the heme iron electronic structure nonequivalence in α- and β-subunits of tetrameric oxy- and deoxyhemoglobins. A comparative study of human, rabbit, and pig oxyhemoglobins with different molecular structure and functions was carried out using Mössbauer spectroscopy with a high velocity resolution [95]. Mössbauer spectra of human, rabbit, and pig oxyhemoglobins measured at 90 K and presented in 1024 channels (Fig. 13.5a–c) were fitted with and without taking into account the heme iron electronic structure nonequivalence in α- and β-subunits. In both cases of spectra fits, small variations of hyperfine parameters were observed (Fig. 13.5d–f). Small differences in quadrupole splitting values of high and low oxygen-affinity human adult deoxyhemoglobin encapsulated in wet silica gel were observed in Ref. 96. However, this result was obtained using Mössbauer spectroscopy with a low velocity resolution (in 256 channels); therefore, the estimated error of 0.02 mm s^{-1} for quadrupole splitting (i.e., probably the error of the fit) was less than the real instrumental error which means that the obtained differences may be doubtful.

A number of Mössbauer studies were related to the analysis of the effect of external factors on hemoglobin. Investigation of oxyhemoglobin radiolysis by γ-rays and electrons and microwave heating was reviewed in Ref. 97. Some differences were shown in the processes of oxyhemoglobin radiolysis related to the type of radiation, its energy, and irradiation dose. The study of conformational changes in methemoglobin and metmyoglobin by low temperature X-ray irradiation was carried out using Mössbauer spectroscopy in Refs. 98,99. Mössbauer spectra showed a reduction of high-spin Fe(III) by thermalized electrons and a production of a metastable low-spin Fe(II) myoglobin and hemoglobin complexes where H_2O was still bound at the sixth coordination.

A comparative Mössbauer study of the effect of phenylhydrazine on normal adult and neonatal red blood cells was carried out in Ref. 100. Although the same total amount of oxidized hemoglobin was found in both cells, a well-defined oxidation product of hemoglobin was demonstrated by Mössbauer spectra only in neonatal cells. This oxidation product was not methemoglobin but a trivalent, high-spin iron compound. Further hemoglobin oxidation by acetylphenylhydrazine was used for diagnostic tests on the basis of Mössbauer spectroscopy [101–104]. It was shown that red blood cells of patients affected by breast cancer are more sensitive to the denaturing action of acetylphenylhydrazine, hence the formation time of hemin, one of the last oxidation products, is significantly shorter then in normal subjects. The experiments showed differences during iron oxidation between breast cancer patients and healthy persons. Different amounts of hemin, after the same incubation time, can discriminate between samples collected from people suffering from cancer and a healthy population.

Human hemoglobin oxidation with Fe(III)-heme formation as a result of the vanadyl ion effect was observed using Mössbauer spectroscopy [105]. Partial oxidation of rat hemoglobin after 70 days of rats feeding with cerium chloride was detected by Mössbauer spectroscopy [106]. An attempt to study hemoglobin from patients with diabetes was done in Ref. 107. However, poor statistical rates, a low signal-to-noise ratio, and a low velocity resolution in these studies did not permit the authors to extract more detailed and exact information.

UNCORRECTED PROOF

CH13 07/04/2013 8:10:52 Page 282

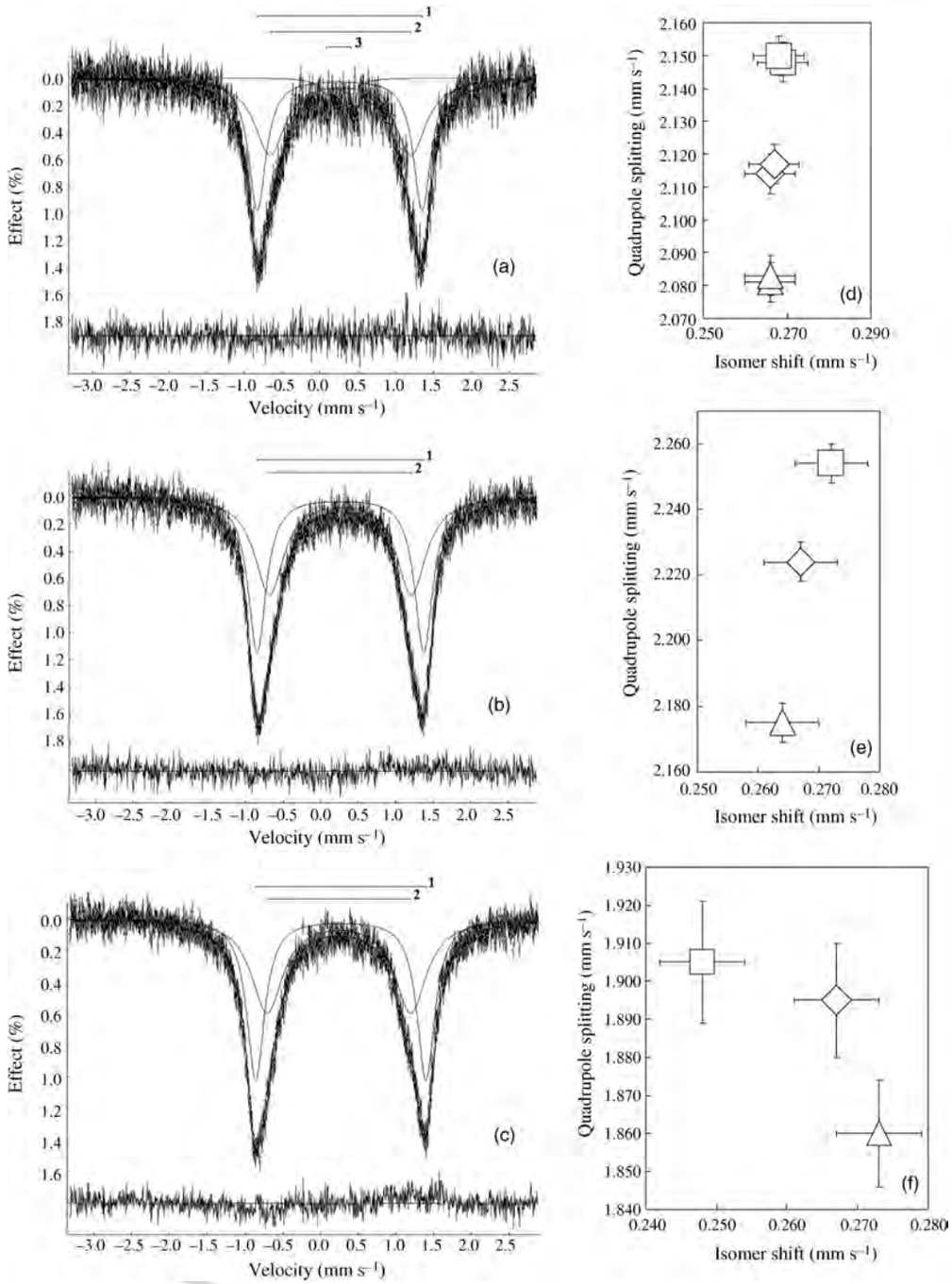

FIGURE 13.5

Mössbauer spectra of normal human adult (a), rabbit (b), and pig (c) oxyhemoglobins measured at 90 K in 4096 channels and presented in 1024 channels (components are the results of the best fit: 1—α-subunits, 2—β-subunits, 3—carboxyhemoglobin) and differences of Mössbauer hyperfine parameters for normal human adult (△), rabbit (◇), and pig (□) oxyhemoglobins at T = 90 K (approximation with one quadrupole doublet (d) and with two quadrupole doublets: for α-subunits (e) and for β-subunits (f); indicated errors are instrumental errors for hyperfine parameters evaluated for the spectra presented in 1024 channels or calculated errors obtained during the spectra fitting if these errors exceeded instrumental errors) [95].

CH13 07/04/2013 8:10:53 Page 283

Recently, measurement of high velocity resolution Mössbauer spectra of oxyhemoglobins from patients with multiple myeloma and chronic myeloleukemia was carried out, and small variations of hyperfine parameters in comparison with normal human adult oxyhemoglobin were revealed [108,109].

13.6 FERRITIN AND HEMOSIDERIN

It is well known that iron in living systems is stored in ferritin and hemosiderin. A number of reviews have been published in the recent years, summarizing the present knowledge about ferritin and hemosiderin [110] and the mineralization process leading to the formation of the iron core [111].

Bauminger and Harrison reviewed studies of the process of iron core formation in human and horse spleen ferritins using Mössbauer spectroscopy. It was demonstrated that iron deposition within ferrihydrite core in human and horse spleen ferritin started with Fe(II) oxidation. This process was associated with ferroxidase center of H-chains. Further, an Fe(III) compound and Fe(III) μ-oxo-bridged dimers in ferroxidase centers of H-chains were found, which were intermediate compounds in the process of iron oxyhydroxide core formation in horse spleen ferritin. The steps leading to ferrihydrite core formation in human L- and H-ferritins were also identified and transfer between ferritin molecules was established [112].

To obtain information about peculiarities of the iron core structure, a number of Mössbauer investigations were undertaken using applied large magnetic fields and low temperatures [113–115]. The influence of the environment on the iron core formation was investigated in bacteria grown in different solutions ($FeSO_4$, $ZnSO_4$, $TbCl_3$) [116] and apoferritin obtained using D_2O or H_2O solution [117]. Another Mössbauer study was undertaken to determine whether or not the iron core formation depends on the oxidant type [118]. Chua-anusorn et al. studied horse spleen apoferritin reconstituted at various temperatures with different numbers of iron atoms per protein shell [119].

Mössbauer spectra of ferritin and hemosiderin from the heart of patients with β-thalassemia/hemoglobin E were obtained in Ref. 120. It was suggested that the iron cores had structures based on the mineral ferrihydrite and were superparamagnetic with a mean blocking temperature of 34 K. The hemosiderin particles had a very poor crystalline structure.

Ferritin contains the polynuclear hydrous ferric oxide core, while iron–polysaccharide complexes modeling ferritin consist of the β-FeOOH core inside the polysaccharide shell instead of the protein shell. These complexes are of particular interest because they are used or being developed as drugs for iron-deficiency anemia treatment [121]. Among them there are iron–dextrin, iron–dextran, iron–polymaltose, and other iron–polysaccharide complexes. Some of these ferritin models were recently studied using Mössbauer spectroscopy [122–129]. Mössbauer spectra of some iron–polysaccharide complexes measured by Funk et al. [123] demonstrated different superparamagnetic behavior and the necessity of several paramagnetic and/or magnetic components for an adequate fit of the spectra. Recently, Oshtrakh et al. carried out a series of comparative studies of small variations in the hyperfine parameters in human liver ferritin and various developed and commercial iron–dextran complexes (IDC) using Mössbauer spectroscopy with a high velocity resolution and spectra presentation in 512 channels [122,124–127]. Small variations of quadrupole splitting were found at 87 K for various IDC and ferritin in frozen solutions and lyophilized forms.

To get a better insight into the issue, Mössbauer spectroscopy with a high velocity resolution was used for a comparative study of human liver ferritin and commercial medicines Imferon (iron–dextran complex), Maltofer®, and Ferrum Lek (iron–polymaltose complexes) [128,129]. Mössbauer spectra of ferritin and its models were measured at 295 K and presented in 4096 or 2048 channels (Fig. 13.6**a**–**d**). The rough fitting of these spectra using one quadrupole split doublet (homogeneous model) demonstrated small differences of hyperfine parameters (Fig. 13.6**e**). It was further observed that the necessary number of quadrupole doublets (heterogeneous model) for the best fit was different for ferritin and its models. For instance, three doublets for Imferon, four doublets for ferritin, and five doublets for Maltofer® and Ferrum Lek were necessary to get the best fit of the spectra measured at 295 K. These differences may be related to structural and/or size variations in the iron cores of the materials studied. The obtained results indicated that the iron core structure in human ferritin and its models is more complicated than it was believed and consists of several regions with structural variations. It was supposed that these regions can be related, for instance, to surface and several internal regions or to the presence of different crystallites.

Papaefthymiou outlined possible directions of future Mössbauer studies in the most recent review [130]. Among them there is a study on magnetic properties that up to now reported about differences in ferritin particles behavior. It is not clear yet whether iron storage conditions and the iron core structure influenced the magnetic properties of ferritin.

CH13 07/04/2013 8:10:53 Page 284

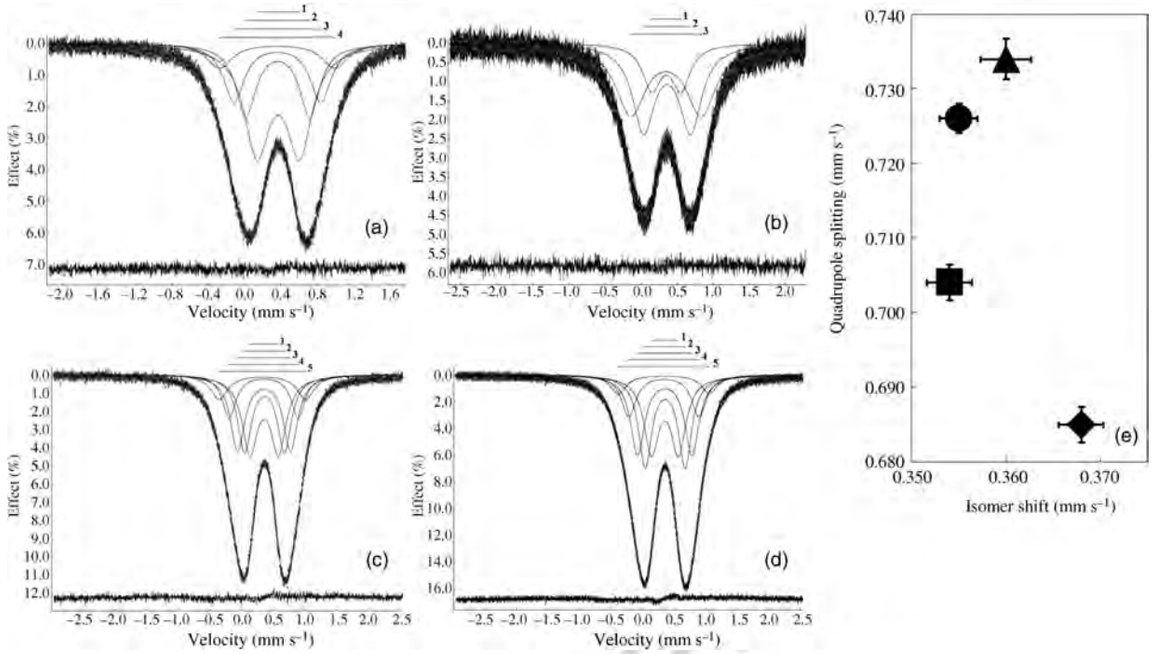

FIGURE 13.6

Mössbauer spectra of human liver ferritin (a), Imferon (b), Maltofer® (c), and Ferrum Lek (d) measured at T = 295 K with a high velocity resolution and presented in 2048 channels (a, b, d) and in 4096 channels (c), indicated components are the results of the best fit; and relationship between the spectral hyperfine parameters for Imferon (■), Maltofer® (▲), Ferrum Lek (●), and human liver ferritin (◆) obtained using one quadrupole doublet fit (**e**) [129].

A further development in the field of Mössbauer spectra fitting and analysis is expected regarding the explanation of applicability of either continuous distributions of quadrupole splitting and hyperfine field or a superposition of discrete quadrupole doublets and magnetic sextets with models of multidomain and multilayer structures of the ferritin iron core. In this case, application of Mössbauer spectroscopy with a high velocity resolution may be used because it leads to a lower instrumental error in the determination of hyperfine parameters (this allows small variations of hyperfine parameters to be distinguished) as well as to a more reliable fitting of complicated Mössbauer spectra (see reviews [32,34–39, 128]).

13.7 TISSUES

Mössbauer studies of tissues containing iron-storage proteins are more complex mainly because of a low iron content in comparison with that in isolated ferritin and hemosiderin. In the first comparative study of purified human liver ferritin, chicken liver and spleen tissues carried out by Oshtrakh et al. [127,131–133], small differences in Mössbauer parameters were observed at 295 K. First, Mössbauer spectra were measured with a high velocity resolution in 4096 channels and presented in 512 channels. Variations of Mössbauer parameters indicated small differences in the iron electronic structure and the iron core structure of the iron-storage proteins. To increase the accuracy and decrease the instrumental error in evaluating the hyperfine parameters, Mössbauer spectra of chicken liver and spleen tissues were measured with a high velocity resolution at 295 K and presented in 1024 channels with fitting using a superposition of two quadrupole doublets within the heterogeneous model (see Fig. 13.7a and b) [133]. Differences in Mössbauer parameters for chicken liver and spleen are clearly seen in Fig. 13.7**c**–**e** and indicate the presence of structural differences in the proteins' iron cores in these tissues.

The possible role of iron in Parkinson's, Alzheimer's, and progressive supranuclear palsy diseases was also studied using Mössbauer spectroscopy. Mössbauer studies demonstrated that the most of iron in the brain including three brain tissues *substantia nigra*, *globus pallidus*, and *hippocampus* was ferritin-like iron [134,135]. The amount of ferritin molecules

CH13 07/04/2013 8:10:53 Page 285

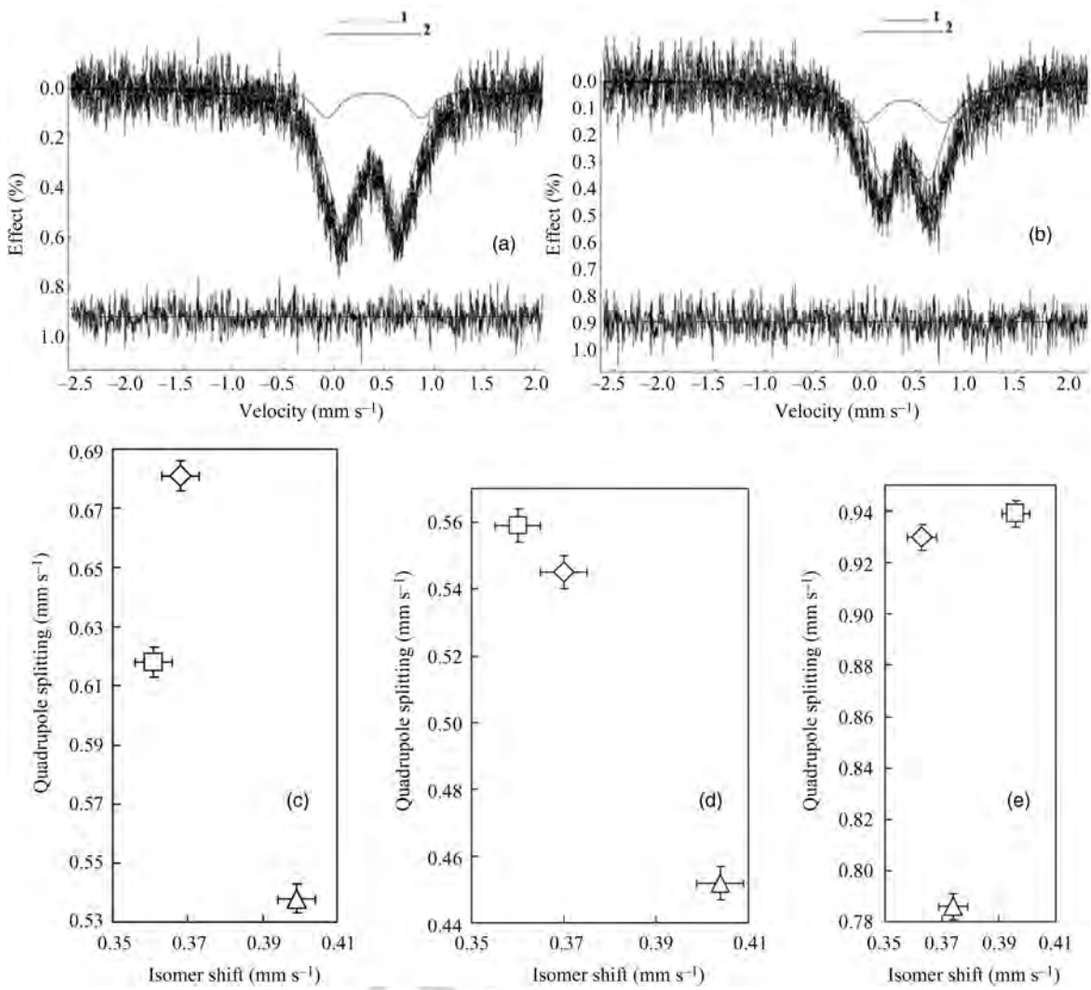

FIGURE 13.7

Mössbauer spectra of chicken liver (a) and spleen (b) tissues measured at 295 K and presented in 1024 channels and differences of Mössbauer hyperfine parameters for normal human liver ferritin (◇), chicken liver (□), and spleen (△) tissues obtained by fitting with one (c) and two (d and e) quadrupole doublets [133].

in Alzheimer's tissues was found to be higher than in control samples, whereas the total amount of iron was the same. It was supposed that either iron cores in Alzheimer's samples were smaller than in the control samples or a great amount of hemosiderin occurs in pathological tissues [136]. The presence of up to 8% of nonferritin-like iron in parkinsonian *substantia nigra* or possible slight differences in the composition of the ferritin-like iron cores in parkinsonian *substantia nigra* were supposed [137]. All Mössbauer spectra measured at 300 and 90 K looked like asymmetric doublets that were fitted using two singlets with the same area and different widths. To assess this asymmetry, the ratio of singlet widths was used referred to as the asymmetry coefficient [138]. However, this approach has no physical meaning. Moreover, there are a number of studies in which asymmetrical Mössbauer spectra of ferritin were fitted using a superposition of several quadrupole doublets [128,129,133].

On the other hand, there are studies presenting an increase of iron concentration in parkinsonian tissues, so this problem remains controversial [139,140]. Such iron increase was associated with neuromelanin, supposed to be the main iron-storage compound in *substantia nigra* neurons. It was believed that a larger cluster size demonstrated by Mössbauer spectroscopy in iron-loaded neuromelanin in comparison with iron-depleted neuromelanin and intact nigral tissue confirmed that additional iron was added to existing iron clusters in neuromelanin.

CH13 07/04/2013 8:10:56 Page 286

Mössbauer study of β-thalassemia/hemoglobin E heart tissue from patients who had received no transfusion and chelation therapy was carried out in Ref. 120. Preliminary results of normal and lymphoid leukemia chicken liver and spleen tissue study using Mössbauer spectroscopy with a high velocity resolution were obtained in Ref. 132. It was observed that Mössbauer hyperfine parameters of liver and spleen samples demonstrated small changes between the corresponding normal and pathological tissues.

13.8 PHARMACEUTICAL PRODUCTS

Various compounds containing Mössbauer isotopes are developed and used in pharmacy. Some diorganotin(IV) compounds with cytotoxic activity against human adenocarcinoma HeLa cells were studied using ^{119}Sn Mössbauer spectroscopy by Ronconi et al. [141]. Xanthopoulou et al. studied organotin(IV) complexes with heterocyclic thioamides with antitumor activity using ^{119}Sn Mössbauer spectroscopy [142]. In addition, some recent studies of tin compounds using ^{119}Sn Mössbauer spectroscopy can be mentioned [143–146]. Gold compounds are also used in pharmacy. Therefore, ^{197}Au Mössbauer spectroscopy was used for the characterization of such compounds. The ^{197}Au Mössbauer spectrum of seleno-auranofin (SeAF), an analogue of auranofin (AF), the orally active antiarthritic gold drug in clinical use, exhibited an asymmetric quadrupole doublet that may be a result of a residual sample texture [147].

Iron-containing pharmaceutical compounds are used and developed as anticancer and antibiotic drugs as well as for treatment of iron deficiency. For instance, Mössbauer spectroscopy was used for studying iron complexes with anticancer antibiotics such as anthracyclines [148], adenosine derivatives [149], and cyclin-dependent kinase inhibitors [150]. Sharaby analyzed iron complexes of hexachlorocyclodiphosph(V)azanes of sulfaguanidine (H_4L) with antimicrobial activity [151]. Recently, some iron-containing complexes with antituberculosis activity were studied using Mössbauer spectroscopy [152,153].

A number of ferric and ferrous compounds are used and developed for treatment of iron-deficiency anemia. The results of Mössbauer studies of ferric complexes with various polysaccharides modeling ferritin [122–129] were considered above. Complex of Fe(III) with protein succinylate was studied in Ref. 154. Recently, a characterization of the iron state in iron–polygalacturonate complex that may be used for iron supplementation was made by Fodor et al. [155]. One ferric and two ferrous compounds in the studied complexes were found. Various vitamins and dietary supplements contain ferrous compounds such as ferrous fumarate, ferrous sulfate, ferrous gluconate, and some others. The studies of the iron in ferrous gluconate demonstrated the presence of a minor ferric compound in addition to ferrous gluconate; moreover, it was shown that Fe^{2+} in both ferrous gluconate and Ascofer® occupied two [156] or three [157] distinct sites. Further studies of vitamins and dietary supplements containing ferrous fumarate, ferrous sulfate, and ferrous chelates were carried out using Mössbauer spectroscopy in Refs 127,158–160. It was found that vitamins and dietary supplements with ferrous fumarate contained minor ferric and ferrous impurities, while those with ferrous sulfate contained minor ferric impurity. In contrast, vitamin and dietary supplement with ferrous iron chelates contained large amount of ferric compounds. Then these studies were continued by measuring Mössbauer spectra with a high velocity resolution [161–163]. The applied experimental technique and the results obtained may be useful and important for controlling the iron state and impurity level in iron-containing medicaments.

13.9 CONCLUSIONS

A brief review of various applications of Mössbauer spectroscopy for biological and biomedical studies demonstrated a high potential of this technique in analyzing various biological and pharmaceutical species containing Mössbauer isotopes. The results obtained are very useful for understanding biological functions of iron-containing biomolecules, the role of iron in the living processes as well as in approaches to understand pathological changes in the living systems, organs, tissues, and biomolecules. It may probably be useful for further development of diagnostically important tests based on Mössbauer spectroscopy. However, this requires improving the quality of Mössbauer spectrometers and spectra measurements. In particular, Mössbauer spectroscopy with a high velocity resolution may be one of further developments of the technique that allows high-quality Mössbauer spectra to be measured, that would be important for biomedical and biological analyses.

UNCORRECTED PROOF

CH13 07/04/2013 8:10:56 Page 287

ACKNOWLEDGMENTS

A.A.K. and K.K. are indebted to Professors A. Vértes, E. Kuzmann, and Z. Homonnay (Budapest) for their invaluable help and many stimulating discussions. M.I.O. and I.V.A. are grateful to Dr. V.A. Semionkin (Ekaterinburg) for his invaluable contribution to biomedical research and development of Mössbauer spectroscopy with a high velocity resolution. A.A.K. gratefully acknowledges support under the NATO "Security through Science" Program (Grants CBP.NR.NREV 981748 and ESP.NR.NRCLG 982857), as well as under the Agreements on Scientific Cooperation between the Russian and Hungarian Academies of Sciences for 2005–2007 (Protocol, Thematic Plan, Project 37), for 2008–2010 (Protocol, Thematic Plan, Project 45), and for 2011–2013 (Protocol, Thematic Plan, Project 28). K.K. gratefully appreciates support by the Hungarian National Science Foundation (OTKA Projects K67835, K68135, NN74045, NN84307) and by the NKTH (Project CZ 11/2007). M.I.O. and I.V.A. are grateful for the basic financing from the Ministry of Science and Education of the Russian Federation. I.V.A. is supported in part by the Ural Federal University Development Program for young scientists financial support

REFERENCES

1. M.I. Oshtrakh, *Mössbauer Effect Ref. Data J.* **2005**, *28*, 273–274.
2. C.E. Johnson, in *Mössbauer Spectroscopy*, U. Gonser, ed., Springer, Berlin, **1975**, pp. 139–166.
3. A. Vértes, L. Korecz, K. Burger, *Mössbauer Spectroscopy*, Elsevier/Akadémiai Kiadó, Amsterdam/Budapest, **1979**, pp. 344–392.
4. K. Spartalian, G. Lang, in *Applications of Mössbauer Spectroscopy*, Vol. 2, R.L. Cohen, ed., Academic Press, New York, **1980**, pp. 249–279.
5. A. Trautwein, E. Bill, in *Transition Metal Chemistry, Proceeding Workshop, Bielefeld, Germany, 14–17 July, 1980*, A. Müller, E. Diemann, eds., Verlag Chemie, Weinheim, **1981**, pp. 239–263.
6. B.H. Huynh, T.A. Kent, *Stud. Phys. Theor. Chem.* **1983**, *25*, 490–560.
7. B.H. Huynh, T.A. Kent, *Adv. Inorg. Biochem.*, **1984**, *6*, 163–223.
8. D.P.E. Dickson, in *Mössbauer Spectroscopy Applied to Inorganic Chemistry*, Vol. *1*, G.J. Long, ed., Plenum Press, New York, **1984**, pp. 339–389.
9. A.X. Trautwein, E. Bill, E.L. Bominaar, H. Winkler, *Struct. Bonding* **1991**, *78*, 1–95.
10. E. Münck, in *Physical Methods in Bioinorganic Chemistry: Spectroscopy and Magnetism*, L. Que Jr., ed., University Science Books, Sausalito, CA, **2000**, pp. 287–319.
11. V. Schünemann, H. Winkler, *Rep. Prog. Phys.* **2000**, *63*, 263–353.
12. H. Paulsen, V. Schünemann, A.X. Trautwein, H. Winkler, *Mössbauer Effect Ref. Data J.* **2005**, *28*, 274–278.
13. D.P.E. Dickson, C.E. Johnson, in *Applications of Mössbauer Spectroscopy*, Vol. 2, P.L. Cohen, ed., Academic Press, New York, **1980**, pp. 209–248.
14. R.I. Mintz, M.I. Oshtrakh, *Arch. Pathol. (Moscow)* **1986**, *48*, 82–87.
15. F. Labenski de Kanter, *Sangre* **1986**, *31*, 187–194.
16. M.I. Oshtrakh, *Hyperfine Interact.* **1991**, *66*, 127–139.
17. M.I. Oshtrakh, *Z. Naturforsch.* **1996**, *51a*, 381–388.
18. M.I. Oshtrakh, *J. Mol. Struct.* **1999**, *480–481*, 109–120.
19. M.I. Oshtrakh, *Spectrochim. Acta Part A* **2004**, *60*, 217–234.
20. M.I. Oshtrakh, *Hyperfine Interact.* **2004**, *159*, 337–343.
21. M.I. Oshtrakh, *Mössbauer Effect Ref. Data J.* **2005**, *28*, 278–283.
22. G.C. Papaefthymiou, *Mössbauer Effect Ref. Data J.* **2005**, *28*, 283–285.
23. I. Ortalli, S. Croci, *Mössbauer Effect Ref. Data J.* **2005**, *28*, 286–287.
24. M.I. Oshtrakh, *Hyperfine Interact.* **2005**, *165*, 313–320.
25. M.I. Oshtrakh, *J. Radioanal. Nucl. Chem.* **2006**, *269*, 407–415.
26. A.A. Kamnev, *J. Mol. Struct.* **2005**, *744–747*, 161–167.
27. A. Nath, *Mössbauer Effect Ref. Data J.* **2007**, *30*, 107–109.
28. Yu.D. Perfiliev, A.A. Kamnev, *Mössbauer Effect Ref. Data J.* **2007**, *30*, 121–122.
29. A.A. Kamnev, in *Metal Ions in Biology and Medicine*, Vol. *10*, P. Collery, I. Maymard, T. Theophanides, L. Khassanova, T. Collery, eds., John Libbey Eurotext, Paris, **2008**, pp. 522–527.

UNCORRECTED PROOF

CH13 07/04/2013 8:10:56 Page 288

30. A. Nath, *J. Nucl. Radiochem. Sci.* **2010**, *11*, A1–A3.
31. A.A. Kamnev, this book, 2013 (Chapter 17).
32. M.I. Oshtrakh, V.A. Semionkin, O.B. Milder, E.G. Novikov, *J. Radioanal. Nucl. Chem.* **2009**, *281*, 63–67.
33. V.A. Semionkin, M.I. Oshtrakh, O.B. Milder, E.G. Novikov, *Bull. Russ. Acad. Sci. Phys.* **2010**, *74*, 416–420.
34. M.I. Oshtrakh, V.A. Semionkin, O.B. Milder, E.G. Novikov, in *Proceeding of the International Conference on the Mössbauer Spectroscopy in Materials Science 2008*, Vol. *1070*, M. Mashlan, R. Zboril, eds., AIP Conference Proceedings, Melville, NY, **2008**, pp. 122–130.
35. M.I. Oshtrakh, V.A. Semionkin, V.I. Grokhovsky, O.B. Milder, E.G. Novikov, *J. Radioanal. Nucl. Chem.* **2009**, *279*, 833–846.
36. M.I. Oshtrakh, V.A. Semionkin, O.B. Milder, E.G. Novikov, *J. Mol. Struct.* **2009**, *924–926*, 20–26.
37. M.I. Oshtrakh, V.A. Semionkin, O.B. Milder, E.G. Novikov, *Bull. Russ. Acad. Sci. Phys.* **2010**, *74*, 407–411.
38. M.I. Oshtrakh, V.A. Semionkin, O.B. Milder, I.V. Alenkina, E.G. Novikov, *Spectrosc. Int. J.* **2010**, *24*, 593–599.
39. M.I. Oshtrakh, I.V. Alenkina, O.B. Milder, V.A. Semionkin, *Spectrochim. Acta Part A* **2011**, *79*, 777–783.
40. H. Paulsen, V. Schünemann, A.X. Trautwein, H. Winkler, *Coord. Chem. Rev.* **2005**, *249*, 255–272.
41. A.A. Kamnev, Chapter 13, in *Plant-Microbe Interactions*, E.A. Barka, C. Clément, eds., Research Signpost, Trivandrum, **2008**, pp. 291–318.
42. A.A. Kamnev, E. Kuzmann, *Polyhedron* **1997**, *16*, 3353–3356.
43. A.A. Kamnev, E. Kuzmann, Yu.D. Perfiliev, Gy. Vankó, A. Vértes, *J. Mol. Struct.* **1999**, *482–483*, 703–711.
44. A.A. Kamnev, E. Kuzmann, *Biochem. Mol. Biol. Int.* **1997**, *41*, 575–581.
45. A.A. Kamnev, A.G. Shchelochkov, Yu.D. Perfiliev, P.A. Tarantilis, M.G. Polissiou, *J. Mol. Struct.* **2001**, *563–564*, 565–572.
46. K. Kovács, A.A. Kamnev, E. Kuzmann, Z. Homonnay, P.A. Szilágyi, V.K. Sharma, A. Vértes, *J. Radioanal. Nucl. Chem.* **2005**, *266*, 513–517.
47. K. Kovács, A.A. Kamnev, J. Mink, Cs. Németh, E. Kuzmann, T. Megyes, T. Grósz, H. Medzihradszky-Schweiger, A. Vértes, *Struct. Chem.* **2006**, *17*, 105–120.
48. K. Kovács, V.K. Sharma, A.A. Kamnev, E. Kuzmann, Z. Homonnay, A. Vértes, *Struct. Chem.* **2008**, *19*, 109–114.
49. R. Raudsepp, I. Arro, *Izv. Akad. Nauk Est. SSR. Fiz. Mat.* **1972**, *21*, 187–192.
50. A.A. Kamnev, E. Kuzmann, in *Spectroscopy of Biological Molecules: Modern Trends. Annex*, P. Carmona, R. Navarro, A. Hernanz, eds., UNED Press, Madrid, **1997**, pp. 85–86.
51. L.O.B. Benetoli, C.M.D. de Souza, K.L. da Silva, I.G. de SouzaJr., H. de Santana, A. PaesanoJr., A.C.S. da Costa, C.T.B.V. Zaia, D.A. M. Zaia, *Orig. Life Evol. Biosph.* **2007**, *37*, 479–493.
52. A. Vértes, D. Nagy, eds., *Mössbauer Spectroscopy of Frozen Solutions*, Akadémiai Kiadó, Budapest, **1990**.
53. A.A. Kamnev, K. Kovács, E. Kuzmann, A. Vértes, *J. Mol. Struct.* **2009**, *924–926*, 131–137.
54. A.A. Kamnev, K. Kovács, A.G. Shchelochkov, L.A. Kulikov, Yu.D. Perfiliev, E. Kuzmann, A. Vértes, in *Metal Ions in Biology and Medicine*, Vol. *9*, M.C. Alpoim, P.V. Morais, M.A. Santos, A.J. Cristóvão, J.A. Centeno, Ph. Collery, eds., John Libbey Eurotext, Paris, **2006**, pp. 220–225.
55. A.A. Kamnev, K. Kovács, R.L. Dykman, E. Kuzmann, A. Vértes, *Bull. Russ. Acad. Sci. Phys.* **2010**, *74*, 394–398.
56. N.I. Chistyakova, V.S. Rusakov, A.A. Shapkin, T.N. Zhilina, D.G. Zavarzina, A. Lančok, J. Kohout, *Mössbauer spectroscopy in materials science-2010*, *AIP Conf. Proc.* **2010**, *1258*, 68–74.
57. N.I. Chistyakova, V.S. Rusakov, K.A. Nazarova, A.A. Shapkin, T.N. Zhilina, D.G. Zavarzina, *J. Phys. Conf. Ser.* **2010**, *217*, 012055.
58. N.I. Chistyakova, V.S. Rusakov, A.A. Shapkin, T.N. Zhilina, D.G. Zavarzina, *Hyperfine Interact.* **2010**, *197*, 325–330.
59. P. Larese-Casanova, S.B. Haderlein, A. Kappler, *Geochim. Cosmochim. Acta* **2010**, *74*, 3721–3734.
60. S.V. Stolyar, O.A. Bayukov, V.P. Ladygina, R.S. Iskhakov, L.A. Ishchenko, V.Yu. Yakovchuk, K.G. Dobretsov, A.I. Pozdnyakov, O.E. Piksina, *Phys. Solid State* **2011**, *53*, 100–104.
61. L.H. Böttger, D. Faivre, D. Schüler, A.X. Trautwein, B.F. Matzanke, *J. Phys. Conf. Ser.* **2010**, *217*, 012020.
62. B.A. Goodman, P.C. DeKock, *J. Plant Nutr.* **1982**, *5*, 345–353.
63. B.A. Goodman, P.C. DeKock, J.D. Rush, *J. Plant Nutr.* **1982**, *5*, 355–362.
64. S. Ambe, *Int. J. Rad. Appl. Instrum. Appl. Radiat. Isot.* **1989**, *40*, 671–675.
65. V. Römheld, H. Marschner, *Adv. Plant. Nutr.* **1986**, *2*, 155–204.
66. S.H. Kilcoyne, P.M. Bentley, P. Tongbai, D.C. Gordon, B.A. Goodman, *Nucl. Instrum. Methods Phys. Res. B* **2000**, *160*, 157–166.
67. N. Rodríguez, N. Menéndez, J. Tornero, R. Amils, V. de la Fuente, *New Phytol.* **2005**, *165*, 781–789.
68. R. Amils, V. de la Fuente, N. Rodríguez, J. Zuluaga, N. Menéndez, J. Tornero, *Plant Physiol. Biochem.* **2007**, *45*, 335–340.
69. W. Schmidt, *Trends Plant Sci.* **2003**, *8*, 188–193.
70. N.J. Robinson, C.M. Procter, E.L. Conolly, M.L. Guerinot, *Nature* **1999**, *397*, 694–697.

UNCORRECTED PROOF

CH13 07/04/2013 8:10:57 Page 289

71. F. Fodor, E. Cseh, A. Varga, Gy. Záray, *J. Plant Nutr.* **1998**, *21*, 1363–1373.
72. K. Kovács, E. Kuzmann, F. Fodor, E. Cseh, Z. Homonnay, A. Vértes, *Hyperfine Interact.* **2008**, *185*, 63–67.
73. K. Kovács, E. Kuzmann, E. Tatár, A. Vértes, F. Fodor, *Planta* **2009**, *229*, 271–278.
74. K. Kovács, E. Kuzmann, F. Fodor, Z. Homonnay, L. Machala, A. Vértes, *J. Phys. Conf. Ser.* **2010**, *217*, 012019.
75. K. Kovács, E. Kuzmann, Z. Homonnay, A. Vértes, L. Gunneriusson, A. Sandström, *Hyperfine Interact.* **2008**, *186*, 69–73.
76. N.D. Chasteen, P.M. Harrison, *J. Struct. Biol.* **1999**, *126*, 182–194.
77. K. Kovács, E. Kuzmann, F. Fodor, A. Vértes, A.A. Kamnev, *Hyperfine Interact.* **2005**, *165*, 289–294.
78. C. Krebs, J.C. Price, J. Baldwin, L. Saleh, M.T. Green, J.M. Bollinger Jr., *Inorg. Chem.* **2005**, *44*, 742–757.
79. I. Gruner, C. Frädrich, L.H. Böttger, A.X. Trautwein, D. Jahn, E. Härtig, *J. Biol. Chem.* **2011**, *286*, 2017–2021.
80. M.-E. Pandelia, W. Nitschke, P. Infossi, M.-T. Giudici-Orticoni, E. Bill, W. Lubitz, *Proc. Natl. Acad. Sci. USA* **2011**, *108*, 6097–6102.
81. M. Lipińska, A. Orzechowska, J. Fiedor, A.I. Chumakov, T. Ślęzak, M. Zając, K. Matlak, J. Korecki, A. Hałas, K. Strzałka, L. Fiedor, K. Burda, *J. Phys. Conf. Ser.* **2010**, *217*, 012021.
82. R. Uebe, B. Voigt, T. Schweder, D. Albrecht, E. Katzmann, C. Lang, L. Böttger, B. Matzanke, D. Schüler, *J. Bacteriol.* **2010**, *192*, 4192–4204.
83. A.J. Panay, M. Lee, C. Krebs, J.M. Bollinger Jr., P.F. Fitzpatrick, *Biochemistry* **2011**, *50*, 1928–1933.
84. F. Bossis, L.L. Palese, *Biochem. Biophys. Res. Commun.* **2011**, *404*, 438–442.
85. M.F. Perutz, G. Fermi, B. Luisi, B. Shaanan, R.C. Liddington, *Acc. Chem. Res.* **1987**, *20*, 309–321.
86. M.F. Perutz, A.J. Wilkinson, M. Paoli, G.G. Dodson, *Ann. Rev. Biophys. Biomol. Struct.* **1998**, *27*, 1–34.
87. V.E. Prusakov, R.A. Stukan, V.I. Gol'danskii, *Biomed. Sci.* **1991**, *2*, 127–134.
88. K. Jiang, I. Ortalli, G. Pedrazzi, X. Zhang, *Phys. Med.* **1993**, *9*, 19–21.
89. M.I. Oshtrakh, *J. Inorg. Biochem.* **1994**, *56*, 221–231.
90. M.I. Oshtrakh, *Z. Naturforsch.* **1998**, *53a*, 608–614.
91. M.I. Oshtrakh, V.A. Semionkin, *Hyperfine Interact.* **2004**, *159*, 345–350.
92. E.I. Yuryeva, M.I. Oshtrakh, *Hyperfine Interact.* **2005**, *165*, 327–331.
93. E.I. Yuryeva, M.I. Oshtrakh, *Bull. Russ. Acad. Sci. Phys.* **2007**, *71*, 1229–1234.
94. E.I. Yuryeva, M.I. Oshtrakh, *Hyperfine Interact.* **2008**, *181*, 37–43.
95. M.I. Oshtrakh, A. Kumar, S. Kundu, A.L. Berkovsky, V.A. Semionkin, *J. Mol. Struct.* **2011**, *993*, 292–296.
96. S. Croci, O.J. Babalola, S. Bettati, C. Valenti, I. Ortalli, F. Parak, *Hyperfine Interact.* **2005**, *165*, 279–283.
97. M.I. Oshtrakh, *Nucl. Instrum. Methods Phys. Res.* **2001**, *B185*, 129–135.
98. S. Croci, A. Dilg, N. Engler, V. Prusakov, O. Iakovleva, I. Ortalli, F. Parak, *Hyperfine Interact. (C)* **2002**, *5*, 237–240.
99. S. Croci, K. Achterhold, I. Ortalli, F.G. Parak, *Hyperfine Interact.* **2008**, *185*, 103–110.
100. Y. Shahal, E.R. Bauminger, E. Zmora, M. Katz, D. Mazor, S. Horn, N. Meyerstein, *Pediatr. Res.* **1991**, *29*, 119–122.
101. S. Croci, I. Ortalli, G. Pedrazzi, G. Passeri, P. Piccolo, *Hyperfine Interact.* **2000**, *126*, 47–52.
102. S. Croci, G. Pedrazzi, G. Passeri, P. Piccolo, I. Ortalli, *Biochim. Biophys. Acta* **2001**, *1568*, 99–104.
103. S. Croci, G. Pedrazzi, G. Passeri, R. Delsignori, I. Ortalli, *Anticancer Res.* **2002**, *22*, 2903–2906.
104. S. Croci, I. Ortalli, G. Pedrazzi, R. Delsignore, G. Passeri, *Hyperfine Interact. (C)* **2002**, *5*, 233–236.
105. D. Xue, J. Lu, K. Wang, *J. Inorg. Biochem.* **1998**, *71*, 79–85.
106. Y. Cheng, Y. Li, R. Li, J. Lu, K. Wang, *Chem. Biol. Interact.* **2000**, *125*, 191–208.
107. A.G. Li, X.B. Ni, Y.W. Cai, G.L. Zhang, H.D. Zhang, Y.X. Ge, *Hejishu (Nuclear Techniques)* **2000**, *23*, 83–85.
108. M.I. Oshtrakh, A.L. Berkovsky, A. Kumar, S. Kundu, A.V. Vinogradov, T.S. Konstantinova, V.A. Semionkin, *Hyperfine Interact.* **2010**, *197*, 301–307.
109. M.I. Oshtrakh, A.L. Berkovsky, A. Kumar, S. Kundu, A.V. Vinogradov, T.S. Konstantinova, V.A. Semionkin, *Biometals* **2011**, *24*, 501–512.
110. E.C. Theil, *Annu. Rev. Nutr.* **2004**, *24*, 327–343.
111. K.J. Hintze, E.C. Theil, *Cell. Mol. Life Sci.* **2006**, *63*, 591–600.
112. E.R. Bauminger, P.M. Harrison, *Hyperfine Interact.* **2003**, *151–152*, 3–19.
113. S. Hackett, W. Chua-anusorn, P. Pootrakul, T.G.St. Pierre, *Biochim. Biophys. Acta* **2007**, *1772*, 330–337.
114. D.E. Madsen, M.F. Hansen, J. Bendix, S. Mørup, *Nanotechnology* **2008**, *19*, 31.
115. G.C. Papaefthymiou, *Nano Today* **2009**, *4*, 438–447.
116. E.R. Bauminger, A. Treffry, M.A. Quail, Z. Zhao, I. Nowik, P.M. Harrison, *Inorg. Chim. Acta* **2000**, *297*, 171–180.

UNCORRECTED PROOF

CH13 07/04/2013 8:10:57 Page 290

117. G.C. Papaefthymiou, A.J. Viescas, R. Horn, E. Carney, G. Zhao, N.D. Chasteen, J. Lee, S.M. Gourn, *Hyperfine Interact.* **2005**, *165*, 333–338.
118. F. Bou-Abdallah, E. Carney, N.D. Chasteen, P. Arosio, A.J. Viescas, G.C. Papaefthymiou, *Biophys. Chem.* **2007**, *130*, 114–121.
119. W. Chua-anusorn, H.R. Mun, J. Webb, N.T. Gorham, T.G.St. Pierre, *Hyperfine Interact.* **2002**, *144/145*, 279–288.
120. W. Chua-anusorn, K.C. Tran, J. Webb, D.J. Macey, T.G.St. Pierre, *Inorg. Chim. Acta* **2000**, *300–302*, 932–936.
121. L.H. Allen, *J. Nutr.* **2002**, *132*, 813–819.
122. M.I. Oshtrakh, V.A. Semionkin, O.B. Milder, A.B. Livshits, A.A. Kozlov, *Z. Naturforsch.* **2000**, *55a*, 186–192.
123. F. Funk, G.J. Long, D. Hautot, R. Büchi, I. Christl, P.G. Weidler, *Hyperfine Interact.* **2001**, *136*, 73–95.
124. M.I. Oshtrakh, V.A. Semionkin, P.G. Prokopenko, O.B. Milder, A.B. Livshits, A.A. Kozlov, *Int. J. Biol. Macromol.* **2001**, *29*, 303–314.
125. M.I. Oshtrakh, O.B. Milder, V.A. Semionkin, P.G. Prokopenko, A.B. Livshits, A.A. Kozlov, A.I. Pikulev, *Z. Naturforsch.* **2002**, *57a*, 566–574.
126. M.I. Oshtrakh, O.B. Milder, V.A. Semionkin, P.G. Prokopenko, L.I. Malakheeva, *Bull. Russ. Acad. Sci. Phys.* **2005**, *69*, 1729–1738.
127. M.I. Oshtrakh, O.B. Milder, V.A. Semionkin, *J. Radioanal. Nucl. Chem.* **2006**, *269*, 547–553.
128. M.I. Oshtrakh, O.B. Milder, V.A. Semionkin, *Hyperfine Interact.* **2008**, *185*, 39–46.
129. M.I. Oshtrakh, I.V. Alenkina, S.M. Dubiel, V.A. Semionkin, *J. Mol. Struct.* **2011**, *993*, 287–291.
130. G.C. Papaefthymiou, *Biochim. Biophys. Acta* **2010**, *1800*, 886–897.
131. M.I. Oshtrakh, O.B. Milder, V.A. Semionkin, P.G. Prokopenko, L.I. Malakheeva, *Hyperfine Interact.* **2004**, *156/157*, 279–284.
132. M.I. Oshtrakh, O.B. Milder, V.A. Semionkin, L.I. Malakheeva, P.G. Prokopenko, *Hyperfine Interact.* **2005**, *165*, 321–326.
133. M.I. Oshtrakh, O.B. Milder, V.A. Semionkin, *Hyperfine Interact.* **2008**, *181*, 45–52.
134. J. Galazka-Friedman, *Hyperfine Interact.* **2008**, *182*, 31–44.
135. J. Galazka-Friedman, A. Friedman, E.R. Bauminger, *Hyperfine Interact.* **2009**, *189*, 31–37.
136. J. Galazka-Friedman, E.R. Bauminger, K. Szlachta, D. Koziorowski, R. Tomasiuk, A. Jaklewicz, Z.K. Wszolek, D. Dickson, K. Kaplinska, A. Friedman, *Acta Physica Polonica* **2011**, *119*, 81–83.
137. J. Galazka-Friedman, E.R. Bauminger, D. Koziorowski, A. Friedman, *Biochim. Biophys. Acta* **2004**, *1688*, 130–136.
138. K. Szlachta, J. Galazka-Friedman, *Acta Physica Polonica* **2011**, *119*, 84–87.
139. L. Zecca, D. Tampellini, M. Gerlach, P. Riederer, R.G. Fariello, D. Sulzer, *J. Clin. Pathol: Mol. Pathol.* **2001**, *54*, 414–418.
140. K.L. Double, M. Gerlach, V. Shünemann, A.X. Trautwein, L. Zecca, M. Gallorini, M.B.H. Youdim, P. Riederer, D. Ben-Shachar, *Biochem. Pharmacol.* **2003**, *66*, 489–494.
141. L. Ronconi, C. Marzano, U. Russo, S. Sitran, R. Graziani, D. Fregona, *J. Inorg. Biochem.* **2002**, *91*, 413–420.
142. M.N. Xanthopoulou, S.K. Hadjikakou, N. Hadjiliadis, M. Schurmann, K. Jurkschat, A. Michaelides, S. Skoulika, T. Bakas, J. Binolis, S. Karkabounas, K. Charalabopoulos, *J. Inorg. Biochem.* **2003**, *96*, 425–434.
143. M. Nath, Sulaxna, X. Song, G. Eng, A. Kumar, *Spectrochim. Acta A, Mol. Biomol. Spectrosc.* **2008**, *70*, 766–774.
144. T.S.B. Baul, A. Paul, L. Pellerito, M. Scopelliti, P. Singh, P. Verma, D. de Vos, *Invest. New Drugs* **2010**, *28*, 587–599.
145. L. Pellerito, C. Prinzivalli, G. Casella, T. Fiore, O. Pellerito, M. Giuliano, M. Scopelliti, C. Pellerito, *J. Inorg. Biochem.* **2010**, *104*, 750–758.
146. G. Ruisi, L. Canfora, G. Bruno, A. Rotondo, T.F. Mastropietro, E.A. Debbia, M.A. Girasolo, B. Megna, *J. Organomet. Chem.* **2010**, *695*, 546–551.
147. D.T. Hill, A.A. Isab, D.E. Griswold, M.J. DiMartino, E.D. Matz, A.L. Figueroa, J.E. Wawro, C. DeBrosse, W.M. Reiff, R.C. Elder, B. Jones, J.W. Webb, C.F. Shaw, *Inorg. Chem.* **2010**, *49*, 7663–7675.
148. H. Drechsel, M.M. Fiallo, A. Garnier–Suillerot, B.E. Matzanke, V. Schünemann, *Inorg. Chem.* **2001**, *40*, 5324–5333.
149. Z. Trávníček, J. Mikulík, M. Čajan, R. Zbořil, I. Popa, *Bioorg. Med. Chem.* **2008**, *16*, 8719–8728.
150. Z. Trávníček, I. Popa, M. Čajan, R. Zbořil, V. Kryštof, J. Mikulík, *J. Inorg. Biochem.* **2010**, *104*, 405–417.
151. C.M. Sharaby, *Spectrochim. Acta A, Mol. Biomol. Spectrosc.* **2005**, *62*, 326–334.
152. S. Melnic, D. Prodius, H. Stoeckli-Evans, S. Shova, C. Turta, *Eur. J. Med. Chem.* **2010**, *45*, 1465–1469.
153. M.B. Tarallo, C. Urquiola, A. Monge, B.P. Costa, R.R. Ribeiro, A.J. Costa-Filho, R.C. Mercader, F.R. Pavan, C.Q.F. Leite, M.H. Torre, D. Gambino, *J. Inorg. Biochem.* **2010**, *104*, 1164–1170.
154. K.B. Raja, S.E. Jafri, D. Dickson, A. Acebròn, P. Cremonesi, G. Fossati, R.J. Simpson, *Pharmacol. Toxicol.* **2000**, *87*, 108–115.
155. J. Fodor, E. Kuzmann, A. Vértes, Z. Homonnay, Z. Klencsár, Z. May, K. Szentmihályi, *Hyperfine Interact.* **2009**, *190*, 283–290.
156. R. Gozdyra, S.M. Dubiel, J. Cieślak, *J. Phys. Conf. Ser.* **2010**, *217*, 012146.
157. S.M. Dubiel, J. Cieślak, R. Gozdyra, *J. Mol. Struct.* **2011**, *991*, 171–177.
158. M.I. Oshtrakh, O.B. Milder, V.A. Semionkin, *Anal. Chim. Acta* **2004**, *506*, 155–160.

UNCORRECTED PROOF

CH13 07/04/2013 8:10:57 Page 291

159. M.I. Oshtrakh, O.B. Milder, V.A. Semionkin, *Hyperfine Interact.* **2004**, *156–157*, 273–277.
160. M.I. Oshtrakh, O.B. Milder, V.A. Semionkin, *J. Pharm. Biomed. Anal.* **2006**, *40*, 1281–1287.
161. M.I. Oshtrakh, V.A. Semionkin, O.B. Milder, E.G. Novikov, *Hyperfine Interact.* **2009**, *190*, 67–74.
162. M.I. Oshtrakh, E.G. Novikov, S.M. Dubiel, V.A. Semionkin, in *Proc. Int. Conf. "Mössbauer Spectroscopy in Materials Science 2010"*, J. Tuček, M. Miglierini, eds., AIP Conference Proceedings, Melville, New York, **2010**, 1258, pp. 75–81.
163. M.I. Oshtrakh, E.G. Novikov, S.M. Dubiel, V.A. Semionkin, *Hyperfine Interact.* **2010**, *197*, 287–294.

UNCORRECTED PROOF